Electronic Supplementary Information (ESI)

Temperature Driven Charge Transfer Process in Quantum Confined Two-Dimensional Mn-doped $CsPbBr_3$ Perovskite Nanoplatelets

Kaliyamoorthy Justice Babu,[a] Ayushi Shukla,[a] Gurpreet Kaur,[a] Arshdeep Kaur,[a] Himanshu Bhatt[a] and Hirendra N. Ghosh*[ab]

[a]Institute of Nano Science and Technology, Mohali, Punjab -160062, India.

[b]Radiation and Photochemistry Division, Bhabha Atomic Research Centre, Mumbai -400085, India.

*Email: hnghosh@inst.ac.in, hnghosh2004@gmail.com, hnghosh@barc.gov.in

Contents

1. Experimental Section

1.1 Chemicals and reagents: Cesium carbonate (Cs_2CO_3, 99% trace metals basis), manganese (II) bromide ($MnBr_2$, 99%), lead (II) bromide ($PbBr_2$, 99.99 % trace metals basis), oleylamine (OLA, tech, 70%), oleic acid (OA, tech, 90%), 1-octadecene (ODE, tech, 90%), N,N'-dimethylformamide (DMF, 99.8%), and methyl acetate (MeOAc, 99.5%) were purchased from Sigma-Aldrich. Acetone (99%, Rankem) and hexane (99.9%, Rankem) solvents were used as obtained. Methyl acetate was used to purify the crude product, and hexane was used to disperse the purified samples. All chemicals were used without further purification.

1.2 Preparation of Mn doped $CsPbBr_3$ Nanoplatelets:

1.2.1 Preparation of Cs-oleate stock solution: 1.25 mmol (~0.2 g) Cs_2CO_3, 10 mL of ODE, and ~0.7 ml of OA was loaded in a 50 mL 3-neck round bottom flask under N_2 environment, and the mixture was degassed with N_2 flow for 30-45 min at 120 °C. The procedure was repeated more than three times to remove the moisture and O_2. After that, the reaction temperature increased to 140 °C for complete dissolution of Cs_2CO_3 under N_2 atmosphere and annealed for 15 min. The reaction mixture turns bright yellow indicating dissolution of the Cs_2CO_3 and formation of the cesium oleate. Finally, the clear and bright yellow reaction mixture was collected through a glass syringe and stored in a deaerated vial sealed with rubber septa. This solution solidified at room temperature and hence, the temperature of the Cs-oleate solution was maintained ~100 °C for the synthesis of $CsPbBr_3$ nanoplatelets.

1.2.2 Synthesis of $CsPbBr_3$ NPLs: $CsPbBr_3$ NPLs were synthesized by following previously reported room temperature approach at ambient condition.[1-2] ODE (5 ml), Cs-oleate (0.4 ml), OA (0.5 ml) and OLM (0.5 ml) were mixed in 50 ml beaker under vigorous stirring. After that, $PbBr_2$ (0.8 ml) (2 mmol in 2 ml DMF) precursor solution was added to the reaction mixture within, 10-15 s. Then, 20 ml of acetone was swiftly injected in the reaction mixture to quench the reaction. The reaction mixture was centrifuged at 8000 rpm for 10 min and then the precipitate was redispersed in 3 ml of hexane. Methyl acetate was added in to the dispersed sample with the ratio of (1:2 v/v ratio of hexane and methyl acetate) then the solution was centrifuged at 6000 rpm for 10 min. The obtained precipitate was redispersed in hexane for further characterization and post synthetic Mn doping.

1.2.3 Synthesis of Mn doped $CsPbBr_3$ NPLs: Synthesis Mn doped $CsPbBr_3$ NPLs were carried out in two steps at room temperature. First, the $CsPbBr_3$ NPLs was prepared as mentioned earlier purified and then redispersed hexane. Next, the appropriate amount of $MnBr_2$ was added and the solution was vigorously stirred. Within 5 min, the blue emission was changed into orange color under UV (365 nm) irradiation. Then the reaction mixture was purified and redispersed in hexane for further study.

2. Instrumentation and sample preparation:

Powder X-ray diffraction measurement (XRD):

Powder XRD was carried out in Rigaku Smart Lab diffractometer operating at 9 kW (200 mA; 45 kV) using Cu–kα (λ=1.54Å) as the incident radiation source. Samples for XRD were prepared by drop casting the nanocrystal solutions on a glass slide to make film under vacuum desiccator.

Transmission Electron Microscopy (TEM) and High-Resolution TEM (HR-TEM):

TEM and HR-TEM images were taken on JEOL JEM 2100 electron microscope operating at an accelerating voltage of 200 kV electron source respectively. TEM samples of were prepared by drop casting of diluted nanocrystals solution in hexane on a carbon-coated copper grid, the grids were dried in air and stored in a vacuum desiccator.

Atomic force microspcopy (AFM) of $CsPbBr_3$ NPLs

The diluted $CsPbBr_3$ NPLs sample was drop casted on Si wafer dried in air and stored in a vacuum desiccator. The AFM measurement has been done using Bruker Multimode 8 scanning probe microscope with a Nanoscope V controller and a J-scanner.

UV-Vis absorption and Photoluminescence (PL) Spectra:

UV-Vis absorption spectra were carried using a Shimadzu UV-2600 spectrophotometer and PL spectra were collected by Edinburgh FS5 spectrofluorometer. The nanocrystal solution dispersed in hexane were taken in cuvette directly for measurement.

2.1 Experimental setup for femtosecond pump probe spectroscopy:

The experimental setup for the acquisition of transient absorption data employs a Ti : Sapphire regenerative amplifier-based femtosecond laser system (Astrella, Coherent systems, central wavelength ~800 nm, energy per pulse ~5 mJ) and Helios Fire spectrometer. The pulse beam from the main laser head with repetition rate of 1 kHz was split into two components, *viz*. pump and probe beam using a dichroic beam splitter (R:T = 90:10). The reflected component i.e. the pump beam can be tuned to any required excitation wavelength (within the predefined system limits, 250 - 1200 nm) using Coherent Inc. based Optical Parametric Amplifier. The pump intensity can be modulated using variable neutral density filter. The other component namely, the probe beam is guided through a computer control-based delay stage onto a CaF_2 window to generate white light continuum. The pump beam is chopped using a synchronized chopper at 500Hz in order to compute the absorbance change in the two consecutive probe pulses which can be defined as $\Delta A = (A^{probe})_{pump\ on} - (A^{probe})_{pump\ off}$. The spectral data obtained is chirped corrected during the analysis to eliminate the group velocity dispersion effects. In order to make certain that there is no contribution from the non-linear processes in the recorded TA spectrum, the TA experiments were conducted by exciting the prepared samples with sufficiently low power intensity (20 $\mu J/cm^2$). All TA experiments were carried out with the sample spin coated on the glass slide (1cmX 1cm) dried in air. The sample coated glass slide mounted inside the cryostat (Pressure < 10^{-6} mbar) (CRYO Industries, USA). Further, the cryostat was placed inside the spectrometer subjected to varied temperatures (5 K, liquid Helium – 300 K, room temperature).

3. Structural Characterization of Mn-doped $CsPbBr_3$ NPLs

XRD patterns:

Powder XRD pattern has been acquired to analyze the phase purity and crystal structure of the as synthesized $CsPbBr_3$ NPLs and Mn-doped $CsPbBr_3$ NPLs. The peak positions of the XRD pattern of $CsPbBr_3$ NPLs consistent with JCPDS (PDF 01-072-7929) value with orthorhombic crystal phase of $CsPbBr_3$ (Fig. S1a).[1,2] After doping with Mn^{2+}, the peak positions of diffraction angle of $CsPbBr_3$ has showed the slight disturbance, which is due to the difference in ionic radius. The peak positions of the 2 theata was shifted slightly to higher angle (magnified Fig.S1b) indicating that the successful incorporation Mn^{2+} in the $CsPbBr_3$ crystal lattice. Moreover, after doping we did not observed the impurity peaks confirming the successful preservation of NPLs.[1,2]

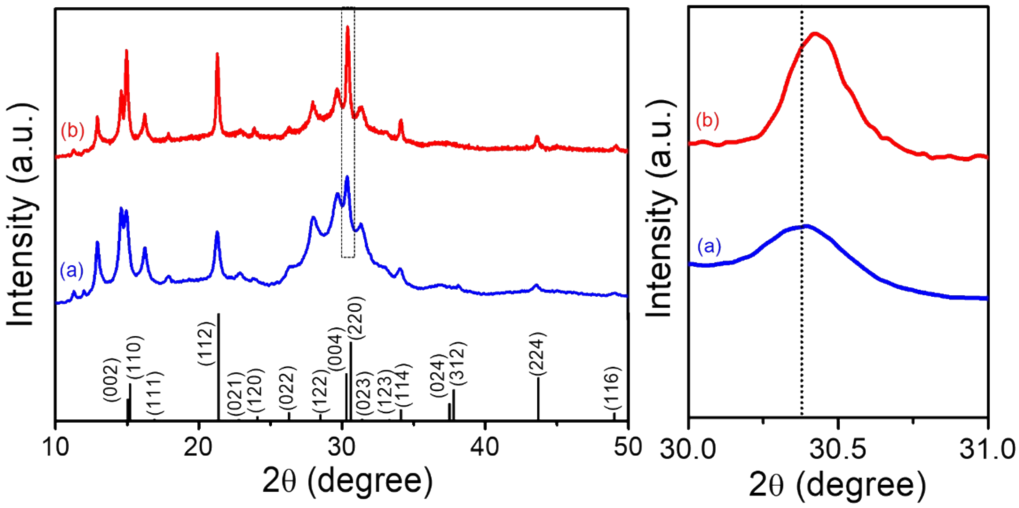

Fig. S1 XRD patterns of (a) $CsPbBr_3$ NPLs and (b) Mn-doped $CsPbBr_3$ NPLs, JCPDF data of orthorhombic phase of $CsPbBr_3$ marked under bottom, Magnified view of the XRD data showing a shift in peak position with Mn doping (right side).

TEM analysis:

Size and morphology of the as synthesized $CsPbBr_3$ NPLs and Mn-doped $CsPbBr_3$ NPLs have been analysed using TEM. HR-TEM image of $CsPbBr_3$ NPLs shows the rectangluar morphology with lateral dimension of 8-10 nm × 40-42 nm (width and length) were observed (Fig. S2a). AFM analysis clearly reveals that the thickness of the NPLs calculate to be 3 nm (inset: Fig S2b), confirming that 5 monolayers of $CsPbBr_3$. Moreover, exciton bohr diameter of $CsPbBr_3$ is ~7 nm, which proved the strong one dimensioanl quantum confinement of synthesized $CsPbBr_3$ NPLs. Interestingly, after Mn^{2+} doping in the $CsPbBr_3$ lattice, the rectangluar morphology has been preseved and maintained the size distribution of NPLs (Fig. S2c). The HR-TEM image of Mn-doped $CsPbBr_3$ NPLs shows the interplanar distance of 0.28 nm, which correspond to (220) plane orthorhombic phase (Fig. S2d).[1,2]

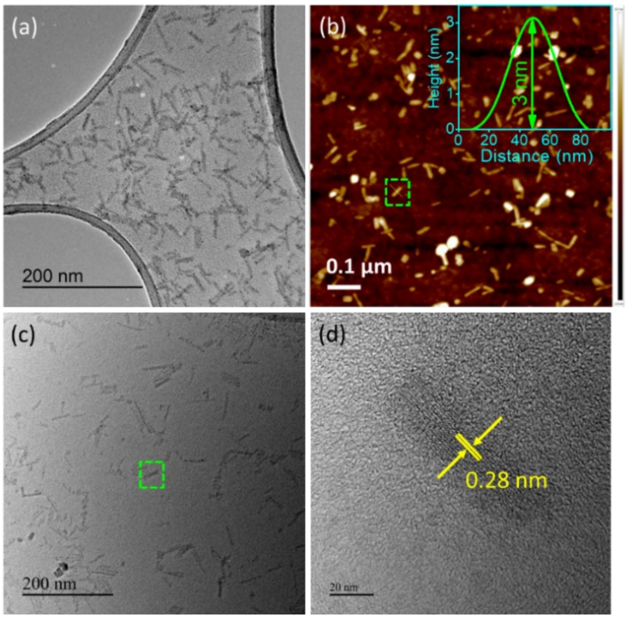

Fig. S2 HR-TEM images of (a) $CsPbBr_3$ NPLs, (b) AFM image of $CsPbBr_3$ NPLs (inset: corresponding height profile) and (c-d) HR-TEM images of Mn-$CsPbBr_3$ NPLs.

XPS analysis:

To confirm the oxidation state of Mn, XPS analysis has been employed for Mn-$CsPbBr_3$ NPLs. From the XPS survey scan Cs, Pb, Br, and Mn elements have been identified (Fig. S3a). To further evaluate the chemical bond formation of the aforementioned elements, XPS scan has been employed. XPS spectrum of Cs 3d showed two prominent peaks with binding energies located at 738 and 724.1 eV, corresponding to the Cs $3d_{3/2}$ and Cs $3d_{5/2}$ levels, respectively (Fig. S3b). For Pb 4f, the XPS peaks located at 142.8 and 138 eV, are ascribed to the $4f_{5/2}$ and

4f$_{7/2}$ levels (Fig. S3c). The Br 3d, binding energies originated at 68.8 and 67.9 eV were assigned to 3d$_{3/2}$ and Br 3d$_{5/2}$ levels, respectively (Fig. S3d).[3] In addition, Fig. S3e showed the two characteristic peaks originated at 641.4 and 653.2 eV corresponding to the 2p$_{3/2}$ and 2p$_{1/2}$, of Mn^{2+}, respectively. The aforementioned binding energies clearly suggest that Mn is in +2 oxidation state, which confirms that Pb^{2+} is replaced by Mn^{2+}. The aforementioned result support that Mn ions are substituted in the CsPbBr$_3$ lattice and preserve the Mn^{2+} state.[4]

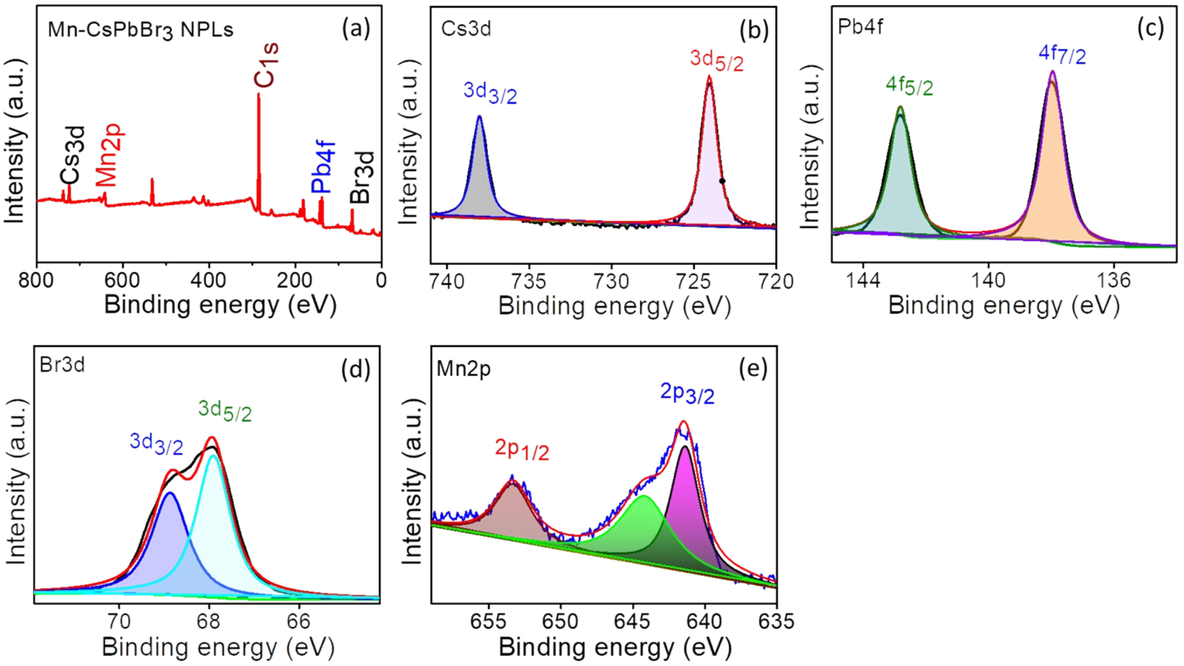

Fig. S3 XPS analysis of Mn-CsPbBr$_3$NPLs: (a) survey scan and high-resolution scans of (b) Cs3d, (c) Pb4f, (d) Br3d and (e) Mn2p.

4. Ultrafast studies:

The TA spectra of CsPbBr$_3$ NPLs exhibit a strong negative peak consistent with exciton bleaching in the 440-460 nm spectral region with a peak maximum of 451 nm (300 K). This strong negative signal is related to the state filling of band-edge exciton and it is exactly coinciding with the steady absorption spectrum. In addition to that, the spectrum also constitutes two positive signals on either side of the bleach. One at red side of the bleach signal peaking at 458-476 nm spectral position with a peak approximately at 464 nm corresponds to the exciton stark effect and it is mainly raised between hot and band edge excitons. Moreover, TA spectra demonstrate the photo induced absorption (PIA) one on the blue side of the spectrum with a broadband signal from 420 to 443 nm, which is ascribed to the forbidden exciton transitions (Fig. S4a,b).[5-9]

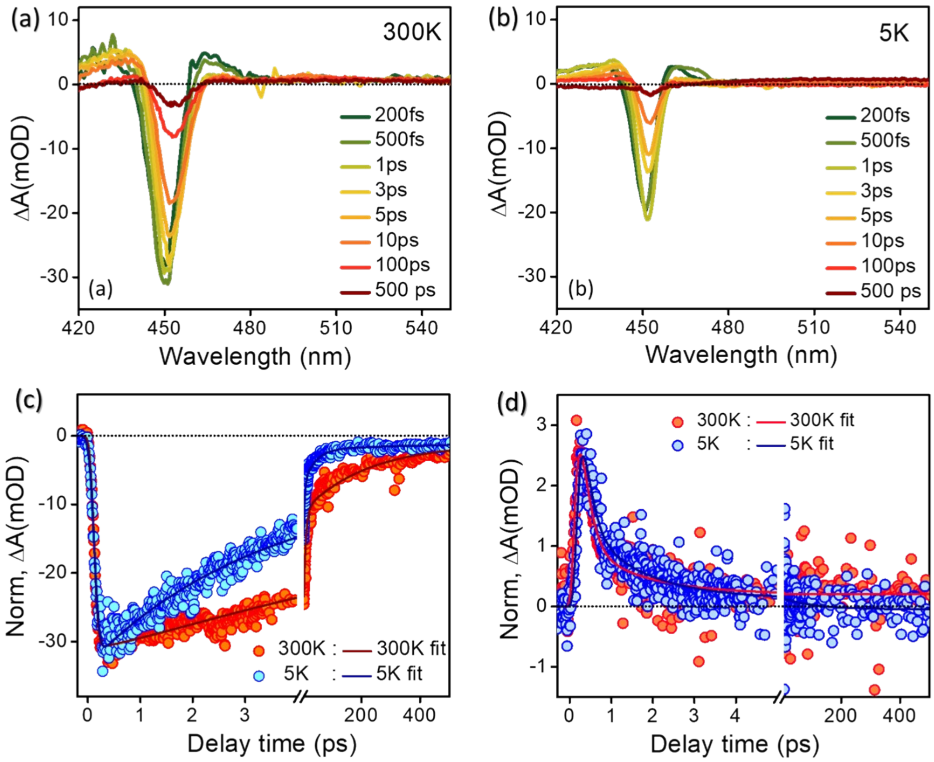

Fig. S4 TA spectra of $CsPbBr_3$ NPLs at (a) 300 K, (b) 5 K; Normalized TA kinetics of $CsPbBr_3$ NPLs monitored in (c) bleach (probe 451 nm) and (d) positive absorption position (probe 464 nm) at 300 K and 5 K under 400 nm pump excitation.

400 nm pump $CsPbBr_3$ NPLs (Kinetics): To investigate the charge carrier dynamics of $CsPbBr_3$ NPLs, TA kinetics were monitored at excitonic bleach position after exciting the sample at 400 nm. Fig 4c,d depicts the temperature dependent transient kinetics monitored at 300 to 5 K. The bleach kinetics of $CsPbBr_3$ NPLs (300-5 K) at 400 nm excitation exhibits the pulse width limited growth.[10] The low-dielectric surrounding of the 2D NPLs leads to reduced screening of the Coulomb-mediated carrier−LO−phonon interaction faster the carrier cooling.

Consequently, the bleach growth (cooling) of the weakly confined $CsPbBr_3$ NCs found to be 0.6 and 0.12 ps for 300 and 5 K, respectively[11] (Table S2). However, decreasing the temperature from 300 to 5 K, we observe a faster recombination suggesting that faster phonon dissipation at lower temperature which facilitates faster recombination.[12,13] Importantly, while decreasing the temperature from 300 to 5 K the transient decay kinetics was completely different and faster that clearly indicates the involement trap states in the temperature dependent TA study. Moreover, the probability of radiative recombination is highly dominant at 5 K than that of non-radiative recombination which results in faster recombination. It has been widely reported that 2D $CsPbBr_3$ NPLs considered by a large surface/volume ratio that resulted in the surface defects due to the vacant sites of Pb^{2+} and Br^{-} ions.[11,14] Interestingly, it is observed that bi-exciton species even at low temperatures cannot be decayed in to single exciton owing to the trapping of charge carriers in the shallow defect states of the NPLs system (Fig S4d) (Table S5).[7-12]

400 nm pump Mn-$CsPbBr_3$ NPLs (Spectra):

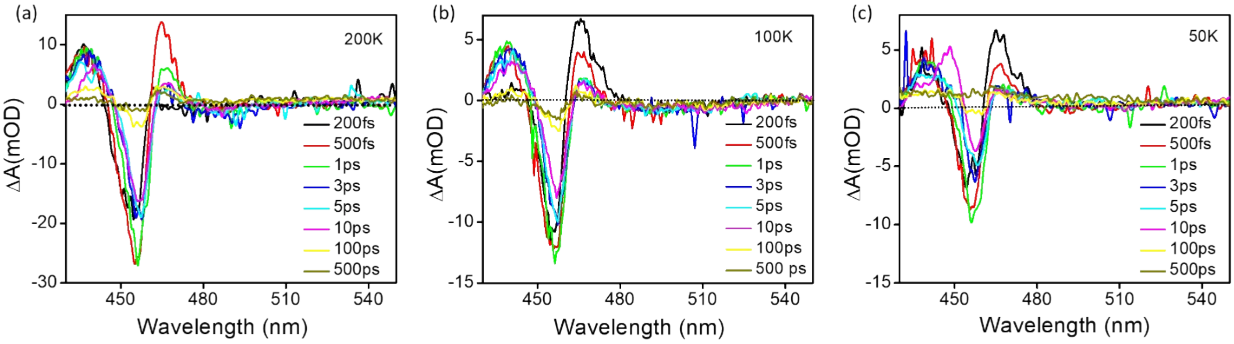

Fig. S5 (a-c) Temperature dependent TA spectra of Mn-$CsPbBr_3$ NPLs under 400 nm pump excitation.

400 nm pump Mn-CsPbBr$_3$ NPLs (Kinetics):

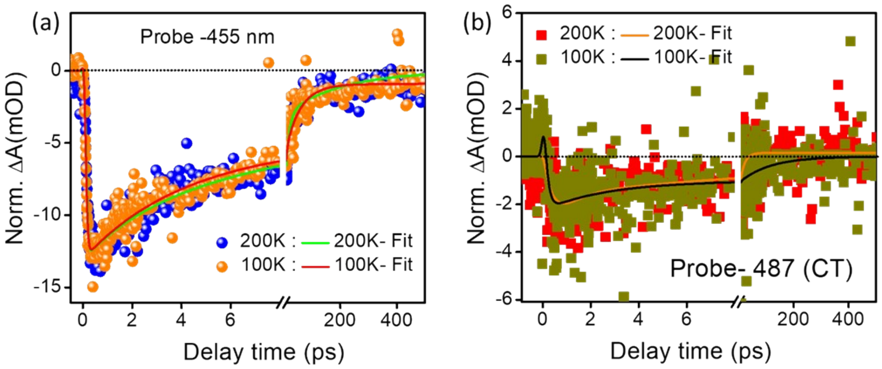

Fig. S6 (a) Normalized TA kinetics of Mn-CsPbBr$_3$ NPLs monitored in (a) bleach and (b) CT positions at different temperatures under 400 nm pump excitation.

Fig. S7 depicts the comparative bleach kinetics of CsPbBr$_3$ NPLs and Mn-CsPbBr$_3$ at 300 K, the bleach recovery kinetics of Mn-CsPbBr$_3$ NPLs was faster than that of CsPbBr$_3$ NPLs, which is due to the participation energy/electron transfer. Moreover, the aforementioned observation matched with our earlier report. Surprisingly, at 5 K the comparative bleach recovery kinetics of CsPbBr$_3$ NPLs and Mn-CsPbBr$_3$ NPLs were similar at early time scale. From the excitonic bleach position kinetics, it is clear that when the temperature is lowerd from 300 to 5 K, charge transfer process predominendly suppressed owing to the trapping of the charge carriers in Br vacancy near to the conduction band state of CsPbBr$_3$ (Fig. 3).[15-22] Thus, at low temperatures, the charge carriers are trapped at a Br vacancy with the energy level close to the conduction band edge and it further formed the bound exciton.[22] Interestingly, the carrier trapping leads to the formation of bound exciton in Mn-CsPbBr$_3$ NPLs and suppress the charge transfer by decreasing the exciton-Mn exchange coupling.[16] So, at lower lattice temperatures the participation of defect states is increased as the carriers are prone to get trapped since the thermal energy is lower which reduces the population of CT states and in turn reduces the charge transfer efficiency at low temperatures. In addition to that, at longer time scale the recovery kinetics of Mn-CsPbBr$_3$ NPLs was completely different and become positive.[22] The aforementioned experimental observation clearly suggest that the charge carriers were trapped in the defect state of Mn-CsPbBr$_3$ NPLs and the same was pictorially represented in Fig 3.

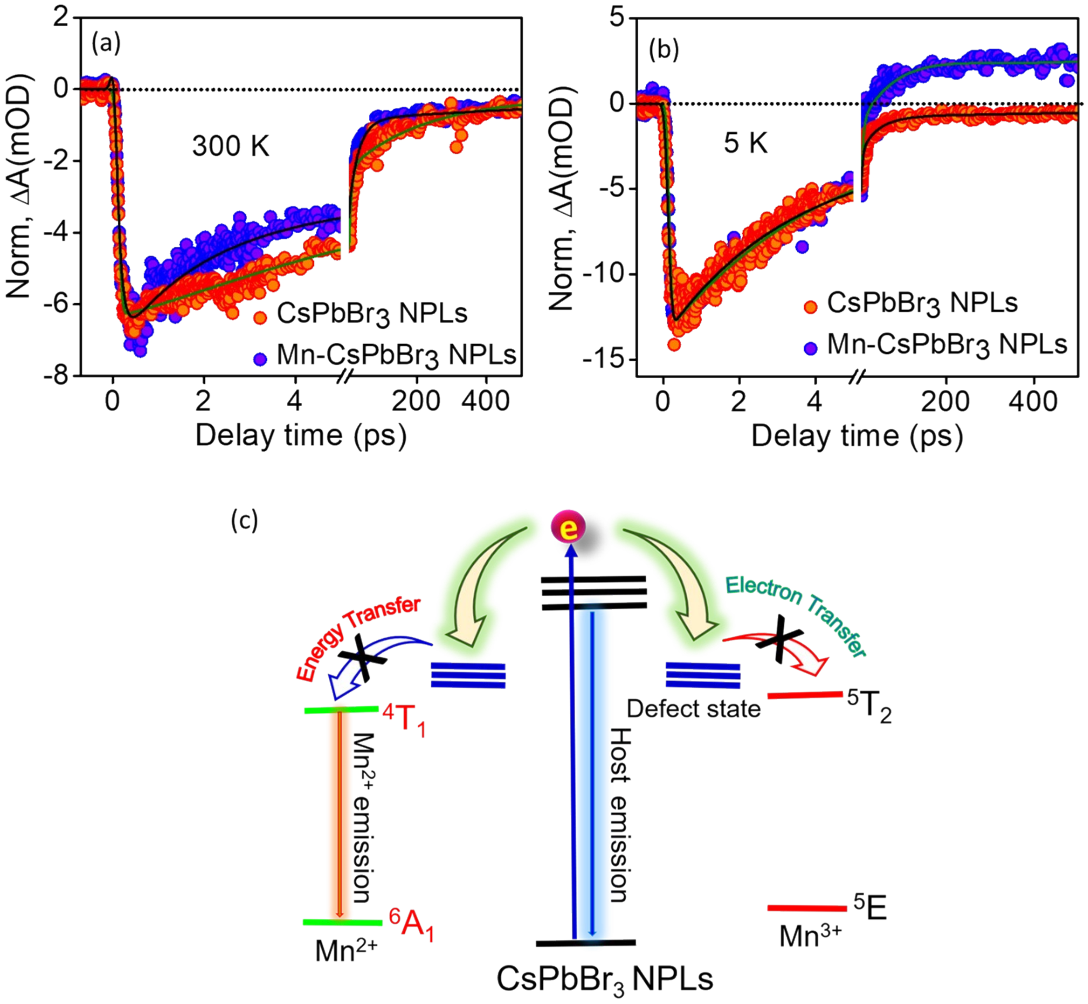

Fig. S7 Comparison of normalized bleach kinetics of $CsPbBr_3$ NPLs and Mn-$CsPbBr_3$ NPLs at (a) 300 K, (b) 5 K after exciting the samples at 400 nm pump. The kinetics were monitored at their bleach maxima and (c) schematic representation depicting the role of temperature in energy and electron transfer in Mn-$CsPbBr_3$ NPLs at 5 K.

Table S1: Details of PL-decay fitting parameters of prepared samples.

System	τ_1 (ns)	A_1 (%)	τ_2 (ns)	A_2 (%)	τ_3 (ns)	A_3 (%)	τ_{avg} (ns)	χ^2
$CsPbBr_3$ NPLs	2.70	45.6	1.25	20.97	0.38	33.43	0.83	1.15
Mn-$CsPbBr_3$ NPLs	8.26	10.5	2.20	52.64	0.70	36.86	1.23	1.12

Table S2: Kinetic fitting parameters at bleach position for $CsPbBr_3$ NPLs deposited over a glass substrate at different temperature under 400 nm pump excitation.

Lattice Temp (K)	τ_g^1	τ_1	τ_2	τ_3
300	<150fs (100%)	7.4ps (-70%)	69ps (-26%)	>1ns (-4%)
200	<150fs (100%)	5 ps (-83.5 %)	280ps (-16.5%)	
100	<150fs (100%)	4.8 ps (-85.6%)	240ps (-14.4%)	
50	<150fs (100%)	5.2 ps (-83.6%)	210ps (-16.4%)	
5	<150fs (100%)	4.5 ps (-83.5%)	190ps (-16.5%)	

Table S3: Kinetic fitting parameters at Bi-exciton position for $CsPbBr_3$ NPLs deposited over a glass substrate at a different temperature under 400 nm pump excitation.

Lattice Temp (K)	τ_g^1	τ_1	τ_2
300	<150 fs (100 %)	420 fs (-83%)	9.8 ps (-17%)
200	<150 fs (100 %)	410 fs (-82.9%)	9.2 ps (-17.1%)
100	<150 fs (100 %)	430 fs (-81.5%)	9.1 ps (-18.5)
50	<150 fs (100 %)	415 fs (-84%)	8.85ps (-16%)
5	<150 fs (100 %)	410fs (-82%)	8.9 ps (-18%)

Table S4: Kinetic fitting parameters at bleach position for Mn-$CsPbBr_3$ NPLs deposited over a glass substrate at different temperature under 400 nm pump excitation.

Lattice Temp (K)	τ_g^1	τ_1	τ_2	τ_3	τ_4
300	<150fs (100%)	0.290 ps (-65%)	69ps (-12%)	380 ps (-18%)	>1ns (-5%)

200	<150fs (100%)	0.25 ps (-74 %)	55 ps (-11%)	250ps (-15%)	
100	<150fs (100%)	0. 23 ps (-79%)	53 ps (11.6%)	240ps (-9.4%)	
50	<150fs (94%)	0. 22 ps (-83.6%)	25 ps (-11.4%)	230 ps (6%)	>1 ns 5%
5	<150fs (83%)	0.18 ps (-66%)	21 ps (-18%)	200 ps 17 %	>1ns -16%

Table S5: Kinetic fitting parameters at CT position for Mn-$CsPbBr_3$ NPLs deposited over a glass substrate at different temperature under 400 nm pump excitation.

Lattice Temp (K)	**τ_g[1]**	**τ_1**	**τ_2**	**τ_3**	**τ_4**
300	0.290 ps (100%)	1.5 (-9%)	8 ps (-41%)	89ps (-44%)	>1 ns (-6%)
200	0.180ps (100%)	0.21 ps (-11 %)	2.1ps (-76.9%)	>70 ps (12.1%)	
100	<0.15ps (100%)	0.21 ps (-11%)	2.1ps (-76.6%)	>66 ps (-12.4%)	
5	<0.15ps (28%)	450 ps (-29%)	8 ps (49%)	320 ps (23%)	>1ns -71%

Notes and references

1 K. J. Babu, G. Kaur, A. Shukla, A. Kaur, T. Goswami, N. Ghorai and H. N. Ghosh, *J. Phys. Chem. Lett.,* 2020, **12,** 302-309.

2 W. J. Mir, Y. Mahor, A. Lohar, M. Jagadeeswararao, S. Das, S. Mahamuni, A. Nag, *Chem. Mater.,* 2018**, 30,** 8170-8178.

3 K. Justice Babu, G. Kaur, A. Shukla, A. Kaur, H. Bhatt, N. Ghorai, G. De, and H. N. Ghosh, 2022. *Mater. Adv.*, 2022, **3,** 6566-6576.

4 J. Chu, Y. Bao, X. Li, F. Gao, and M. Wang, *Steel Res. Int.*, 2021, **92,** 2000333.

5 Q. Li, and T. Lian, *J. Phys. Chem. Lett.,* 2019, **10,** 566-573.

6 B. R. Vale, E. C. Socie, A. Burgos-Caminal, J. Bettini, M. A. Schiavon, and J. E. Moser, *J. Phys. Chem. Lett.,* 2020, **11,** 387-394.

7 E. Socie, B. R. Vale, A. Burgos-Caminal, and J. E. Moser, *Adv. Opt. Mater.,* 2021. **9,** 2001308.

8 W. Tao, C. Zhang, Q. Zhou, Y. Zhao, and H. Zhu, *Nature Commun.*, 2021, **12,** 1-8.

9 G. Kaur, K. J. Babu, N. Ghorai, T. Goswami, S. Maiti and H. N. Ghosh, *J. Phys. Chem. Lett.,* 2019, **10,** 5302−5311.

10 V. A. Hintermayr, L. Polavarapu, A. S. Urban, and J. Feldmann, *ACS Nano*, 2018, **12,** 10151-10158.

11 K. Justice Babu, G. Kaur, A. Shukla, R. Saha, A. Kaur, M. S. Deva, D. K. Yadav and H. N. Ghosh, *ACS Photonics,* 2022, **9, 3,** 969–978.

12 S. Peng, Q. Wei, B. Wang, Z. Zhang, H. Yang, G. Pang, K. Wang, G. Xing, X. W. Sun, and Z. Tang, *Angew. Chem. Int. Ed.,* 2020, **59,** 22156-22162.

13 S. J. Vonk, M. B. Fridriksson, S. O. Hinterding, M. J. Mangnus, T. P. Van Swieten, F. C. Grozema, F. T. Rabouw, and W. Van Der Stam, *J. Phys. Chem. C,* 2020, **124,** 8047-8054.

14 S. M. Lee, C. J. Moon, H. Lim, Y. Lee, M. Y. Choi, and J. Bang, *J. Phys. Chem. C,* 2017, **121,** 26054-26062.

15 V. Pinchetti, A. Anand, Q. A. Akkerman, D. Sciacca, M. Lorenzon, F. Meinardi, M. Fanciulli, L. Manna, and S. Brovelli, *ACS Energy Lett.*, 2018, **4,** 85-93.

16 D. Rossi, D. Parobek, Y. Dong, and D. H. Son, *J. Phys. Chem. C,* 2017, **121,** 17143−17149.

17 M. Sebastian, J. A. Peters, C. C. Stoumpos, J. Im, S. S. Kostina, Z. Liu, M. G. Kanatzidis, A. J. Freeman, and B. W. Wessels, *Phys. Rev. B,* 2015, **92,** 235210.

18 K. R. Pradeep, A. Elumalai, and R. Viswanatha, *J. Phys. Chem. C,* 2022,**126**, 23, 9813–9819.

19 B. P. Kore, S. Das, and D. D. Sarma, *J. Chem. Sci.,* 2021, **133,** 1-13.

20 H. Zhang, J. Yao, K. Zhou, Y. Yang, and H. Fu, *Chem. Mater.,* 2022, **34,** 1854-1861.

21 S. Yu, J. Xu, X. Shang, E. Ma, F. Lin, W. Zheng, D. Tu, R. Li, and X. Chen, *Adv. Sci.*, 2021, **8,** 2100084.

22 G. Kaur, K. J. Babu, and H. N. Ghosh, *J. Phys. Chem. Lett.,* 2020, **11,** 6206-6213.